Electronic Supplementary Material (ESI) for Dalton Transactions.
This journal is © The Royal Society of Chemistry 2022

Electronic Supplementary Information (ESI)

S-Heptazine N-Ligand Based Luminescent Coordination Materials: Synthesis, Structural and Luminescent Studies of Lanthanide-Cyamelurate Networks

Mohamed Essalhi,[a] Midhun Mohan,[a] Gabriel Marineau-Plante,[b] Adrien Schlacter,[b] Thierry Maris,[c] Pierre D. Harvey*[b] and Adam Duong*[a]

[a] *Département de Chimie, Biochimie et physique, Institut de Recherche sur l'Hydrogène and Laboratory of Functional Materials for Energy and Nanotechnology (DuongLab), Université du Québec à Trois-Rivières, Trois-Rivières, Québec, G9A 5H7, Canada*

[b] *Département de chimie, Université de Sherbrooke, Sherbrooke, PQ, J1K 2R1, Canada*

[c] *Département de Chimie, Université de Montréal, Montréal, Québec, H3C 3J7, Canada*

*To whom correspondence should be addressed. E-mail: adam.duong@uqtr.ca

Contents

Figure S1. a) Thermal atomic displacement ellipsoid plot of the asymmetric unit of Dy-**Cy** from Ln-**Cy** series 1. The ellipsoids of non-hydrogen atoms are drawn at 50% probability level, and hydrogen atoms are represented by a sphere of arbitrary size. b) Coordination environment for Dy ion center in the crystal structure of Dy-**Cy** from Ln-**Cy** series 1..... 5

Figure S2. a) Thermal atomic displacement ellipsoid plot of the asymmetric unit of Ho-**Cy** from Ln-**Cy** series 2. The ellipsoids of non-hydrogen atoms are drawn at 50% probability level, and hydrogen atoms are represented by a sphere of arbitrary size. b) Coordination environment for Ho ion center in the crystal structure of Ho-**Cy** from Ln-**Cy** series 2..... 6

Figure S3. a) Thermal atomic displacement ellipsoid plot of the asymmetric unit of Ln-**Cy** series 3 (Ln = Ce). The ellipsoids of non-hydrogen atoms are drawn at 50% probability level, and hydrogen atoms are represented by a sphere of arbitrary size. b)

Coordination environment for Ln center in the crystal structure of Ln-**Cy** series 3 (Ln = Ce). 7

Figure S4. a) Thermal atomic displacement ellipsoid plot of the asymmetric unit of the Ln-**Cy** series 4 (Ln = La). The ellipsoids of non-hydrogen atoms are drawn at 50% probability level, and hydrogen atoms are represented by a sphere of arbitrary size. b) Coordination environment for Ln center in the crystal structure of Ln-**Cy** series 4 (Ln = La). 8

Table S1. Crystal data and structure refinement for Ln-**Cy** (series 1). 9

Table S2. Crystal data and structure refinement for Ln-**Cy** (series 2). 10

Table S3. Crystal data and structure refinement for Ce-**Cy** (series 3). 11

Table S4. Crystal data and structure refinement for La-**Cy** (series 4). 12

Table S5. Effective ionic radii (Å) of Ln^{3+} ions with corresponding coordination number (Shannon-Prewitt data). 12

Figure S5. Effective ionic radius (Å) vs Ln^{3+} ions (cn = coordination number). 13

Figure S6. Two-dimensional fingerprint plots of the Ln-**Cy** series 1. 14

Figure S7. Two-dimensional fingerprint plots of Ln-**Cy** series 2. 14

Figure S8. Two-dimensional fingerprint plots of Ln-**Cy** series 3. 15

Figure S9. Two-dimensional fingerprint plots of Ln-**Cy** series 4. 15

Figure S10. FTIR spectra of Ln-**Cy** series 1 in comparison with potassium cyamelurate. 16

Figure S11. FTIR spectra of Ln-**Cy** series 2 in comparison with potassium cyamelurate. 16

Figure S12. FTIR spectra of Ln-**Cy** series 3 in comparison with potassium cyamelurate. 17

Figure S13. FTIR spectra of Ln-**Cy** series 4 in comparison with potassium cyamelurate. 17

Figure S14. Experimental and simulated PXRD patterns for La-**Cy** compound. 18

Figure S15. Experimental and simulated PXRD patterns for Ce-**Cy** compound..... 18

Figure S16. Experimental and simulated PXRD patterns for Ln-**Cy** series 1. 19

Figure S17. Experimental and simulated PXRD patterns for Ln-**Cy** series 2. 19

Figure S18. Thermogravimetric analysis curves for Ln-**Cy** series 1. 20

Figure S19. Thermogravimetric analysis curves for Ln-**Cy** series 2. 20

Figure S20. Thermogravimetric analysis curve for Ln-**Cy** series 3..... 21

Figure S21. Thermogravimetric analysis curve for Ln-**Cy** series 4..... 21

Figure S22. Absorption (black), emission (red) and excitation (blue) spectra for K_3**Cy** in solution in water at 298 K (λ_{ex} = 270 nm, λ_{em} = 364 nm). The weak signal at ~305 nm is suspected to be fluorescence, and the large and intense one centered at 364 nm is assigned to a triplet emission. Unfortunately, the ligand decomposes upon laser exposure at 266 nm, so the fluorescence lifetime is not accessible. 22

Figure S23. Side and front view of geometry optimization for **Cy**$^{3-}$ anion in the gas phase. 22

Table S6. Cartesian coordinates (Å) of the geometry optimized **Cy**$^{3-}$ in the gas phase.. 23

Table S7. Calculated position, oscillator strength (f) and major contributions (%) of the first 100 singlet-singlet electronic transitions for **Cy**$^{3-}$ in the gas phase. 23

Figure S24. Simulated absorption spectrum for **Cy**$^{3-}$ in the gas phase by TDDFT computations. Bar graph reporting the calculated oscillator strength and the calculated position of the 100th electronic transitions calculated by TDDFT for **Cy**$^{3-}$ in the gas phase (bar graph; f = computed oscillator strength). 27

Figure S25. Solid-state absorption (black), emission (red) and excitation (blue) spectra for La-**Cy** at 298 K (λ_{ex} = 270 nm, λ_{em} = 335 nm) and 77K (λ_{ex} = 270 nm, λ_{em} = 355 nm). 28

Figure S26. Decay of emission intensity, fit, IRF and residual of Gd-**Cy** at 298 K. λ = 339 nm (λ_{ex} = 277 nm), τ_e {f%} = 15 μs {100}, χ^2 = 1.070..... 28

Figure S27. Solid-state absorption (black), emission (red) and excitation (blue) spectra for Sm-**Cy** at 77K (λ_{ex} = 290 nm, λ_{em} = 643 nm)..... 29

Figure S28. Solid-state absorption (black), emission (red) and excitation (blue) spectra for Eu-**Cy** at 77K (λ_{ex} = 300 nm, λ_{em} = 615 nm). 29

Figure S29. Decay of emission intensity, fit, IRF and residual of Eu-**Cy**. Left at 77 K λ = 615 nm (λ_{ex} = 300 nm), τ_e {f%} = 16 μs {100}, χ^2 = 1.001..... 30

Figure S31. Decay of emission intensity, fit, IRF and residual of Tb-**Cy**. Left, at 77 K λ = 620 nm (λ_{ex} = 270 nm), τ_e {f%} = 50 μs {100}, χ^2 = 1.031..... 31

Figure S32. Solid-state absorption (black), emission (red) and excitation (blue) spectra for Dy-**Cy** at 298 K (λex = 270 nm, λem = 571 nm) and 77K (λex = 270 nm, λem = 575 nm). 31

Figure S33. Decay of emission intensity, fit, IRF and residual of Dy-**Cy** at 298 K. λ = 570 nm (λ_{ex} = 270 nm), τ_e {f%} = 3.48 μs {100}, χ^2 = 1.034..... 32

Figure S34. Solid-state absorption (black), emission (red) and excitation (blue) spectra for Er-**Cy** at 298 K (λ_{ex} = 300 nm, λ_{em} = 336 nm). 32

Figure S35. Solid-state absorption (black) spectra for Ce-**Cy** at 298 K. 33

Figure S36. Solid-state absorption (black) spectra for Pr-**Cy-** at 298 K. 33

Figure S37. Solid-state absorption (black) for Ho-**Cy** at 298 K. 34

Table S8. Photophysical properties of all emissive Ln-**Cy**. 34

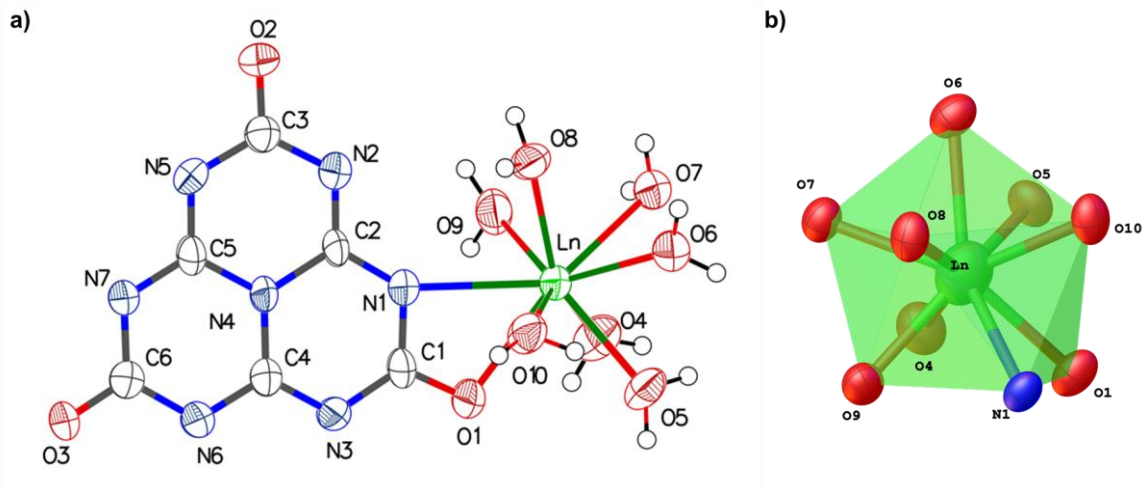

Figure S1. a) Thermal atomic displacement ellipsoid plot of the asymmetric unit of Dy-**Cy** from Ln-**Cy** series 1. The ellipsoids of non-hydrogen atoms are drawn at 50% probability level, and hydrogen atoms are represented by a sphere of arbitrary size. b) Coordination environment for Dy ion center in the crystal structure of Dy-**Cy** from Ln-**Cy** series 1.

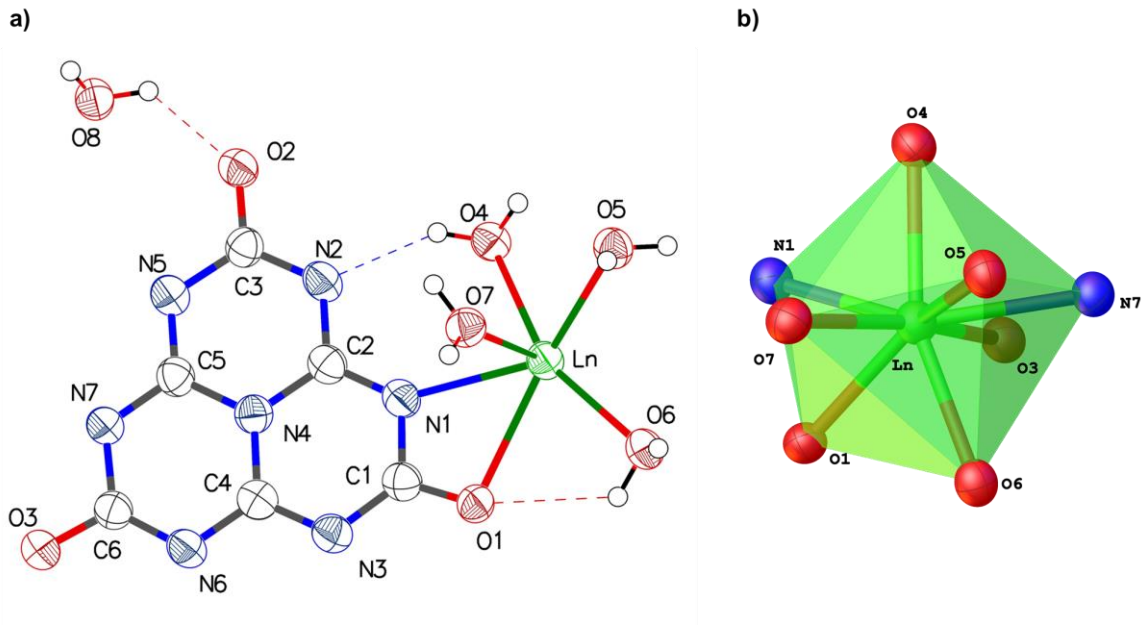

Figure S2. a) Thermal atomic displacement ellipsoid plot of the asymmetric unit of Ho-**Cy** from Ln-**Cy** series 2. The ellipsoids of non-hydrogen atoms are drawn at 50% probability level, and hydrogen atoms are represented by a sphere of arbitrary size. b) Coordination environment for Ho ion center in the crystal structure of Ho-**Cy** from Ln-**Cy** series 2.

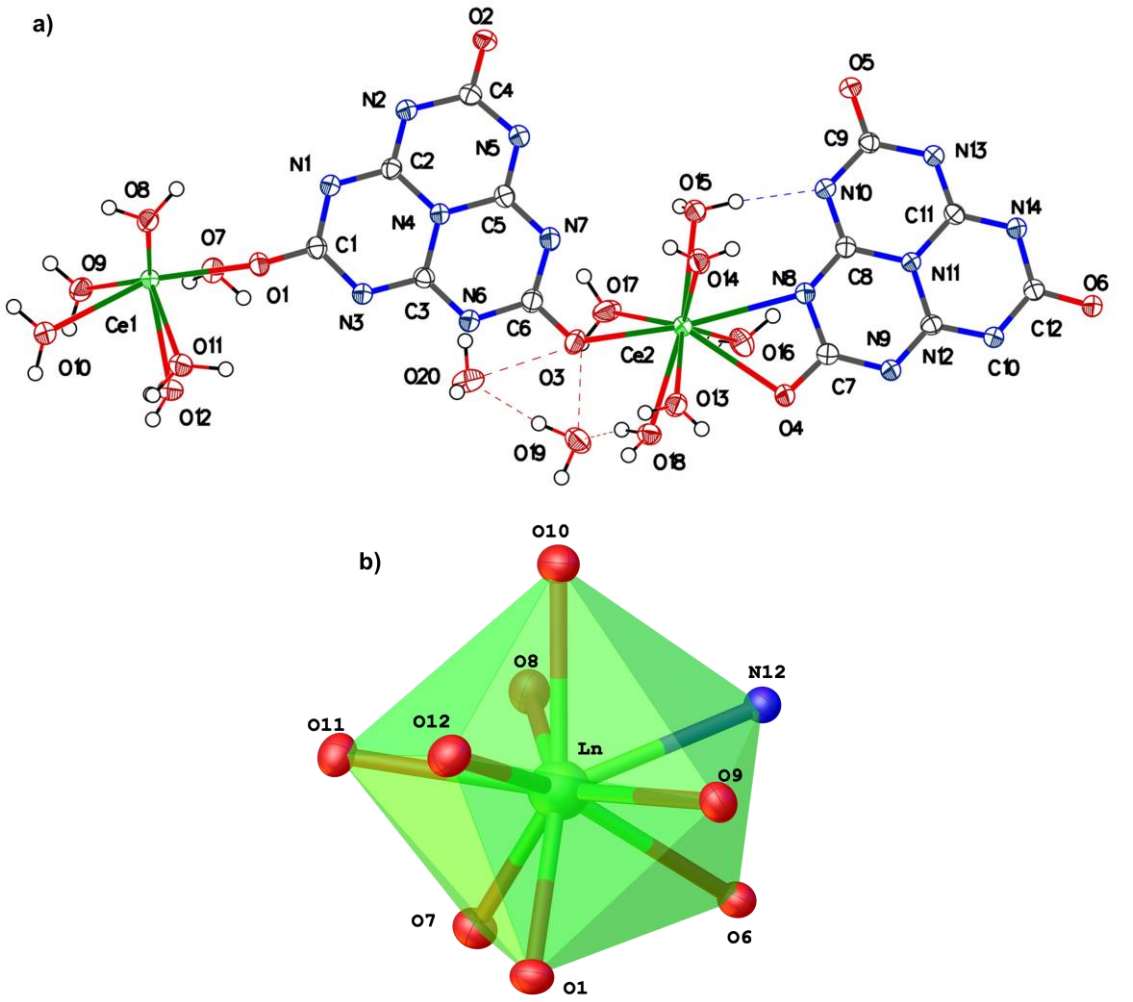

Figure S3. a) Thermal atomic displacement ellipsoid plot of the asymmetric unit of Ln-**Cy** series 3 (Ln = Ce). The ellipsoids of non-hydrogen atoms are drawn at 50% probability level, and hydrogen atoms are represented by a sphere of arbitrary size. b) Coordination environment for Ln center in the crystal structure of Ln-**Cy** series 3 (Ln = Ce).

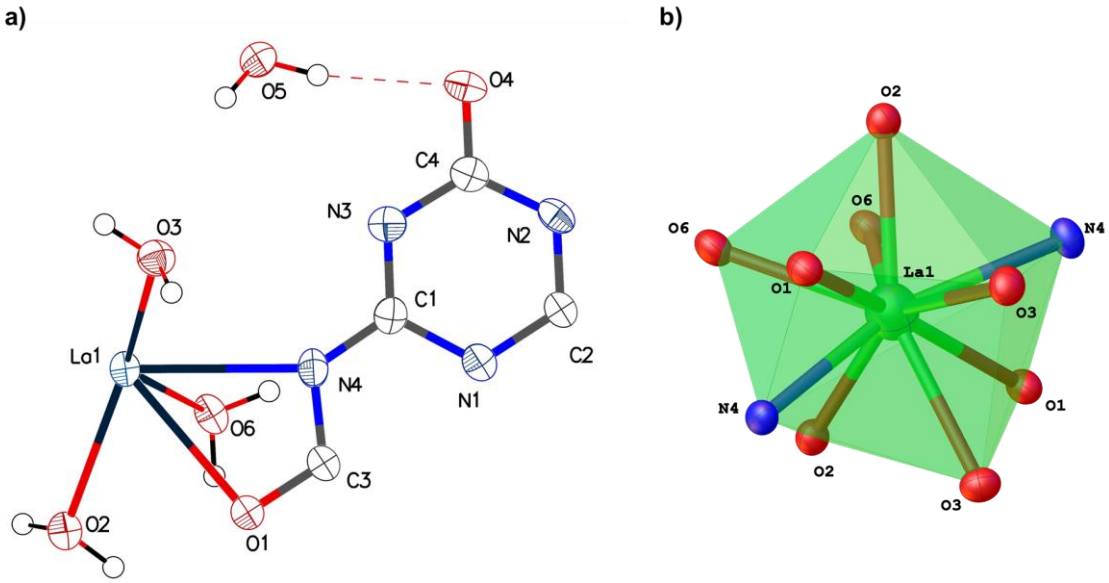

Figure S4. a) Thermal atomic displacement ellipsoid plot of the asymmetric unit of the Ln-**Cy** series 4 (Ln = La). The ellipsoids of non-hydrogen atoms are drawn at 50% probability level, and hydrogen atoms are represented by a sphere of arbitrary size. b) Coordination environment for Ln center in the crystal structure of Ln-**Cy** series 4 (Ln = La).

Table S1. Crystal data and structure refinement for Ln-**Cy** (series 1).

Identification code	**Sm-Cy**	**Eu-Cy**	**Tb-Cy**	**Dy-Cy**
Empirical formula	$C_6H_{14}N_7O_{10}Sm$	$C_6H_{14}N_7O_{10}Eu$	$C_6H_{14}N_7O_{10}Tb$	$C_6H_{14}N_7O_{10}Dy$
CCDC number	2178361	2178362	2178359	2178360
Formula weight	494.59	496.20	503.16	506.74
Temperature/K	298	295	298	295
Crystal system	monoclinic	monoclinic	monoclinic	monoclinic
Space group	$P2_1/n$	$P2_1/n$	$P2_1/n$	$P2_1/n$
a/Å	11.9028(6)	11.8872(6)	11.8582(4)	11.8401(11)
b/Å	6.8680(3)	6.8605(3)	6.8416(2)	6.8183(7)
c/Å	16.7913(8)	16.7718(8)	16.6967(5)	16.6650(16)
α/°	90	90	90	90
β/°	93.617(2)	93.608(2)	93.700(1)	93.753(4)
γ/°	90	90	90	90
Volume/Å^3	1369.93(11)	1365.07(11)	1351.76(7)	1342.5(2)
Z	4	4	4	**2 4**
ρ_{calc}g/cm^3	2.398	2.414	2.472	2.507
μ/mm^{-1}	32.936	33.639	26.484	30.541
F(000)	964.0	968.0	976.0	980.0
Radiation	CuKα (λ = 1.54178)	CuKα (λ = 1.54178)	CuKα (λ = 1.54178)	CuKα (λ = 1.54178)
2Θ range for data collection/°	8.848 to 140.184	8.86 to 141.39	8.882 to 140.274	8.892 to 140.642
Reflections collected	35375	23809	24483	18994
Independent reflections	2614 [R_{int} = 0.0372, R_{sigma} = 0.0135]	2598 [R_{int} = 0.0440, R_{sigma} =0.0222]	2561 [R_{int} = 0.0402, R_{sigma} = 0.0213]	2503 [R_{int} = 0.0752, R_{sigma} =0.0442]
Goodness-of-fit on F^2	1.036	1.043	1.053	1.108
Final R indexes [I>=2σ (I)]	R_1 = 0.0206, wR_2 = 0.0571	R_1 = 0.0331, wR_2 = 0.0769	R_1 = 0.0248, wR_2 = 0.0616	R_1 = 0.0714, wR_2 = 0.1944
Final R indexes [all data]	R_1 = 0.0207, wR_2 = 0.0571	R_1 = 0.0339, wR_2 = 0.0774	R_1 = 0.0265, wR_2 = 0.0626	R_1 = 0.0787, wR_2 = 0.2056

Table S2. Crystal data and structure refinement for Ln-**Cy** (series 2).

Identification code	**Ho-Cy**	**Er-Cy**	**Yb-Cy**
Empirical formula	$C_6H_{10}N_7O_8Ho$	$C_6H_{10}N_7O_8Er$	$C_6H_{10}N_7O_8Yb$
CCDC number	2178364	2178356	2178363
Formula weight	946.28	475.47	481.25
Temperature/K	298	100	100
Crystal system	monoclinic	monoclinic	monoclinic
Space group	Cc	Cc	Cc
a/Å	5.7138(3)	5.69360(10)	5.6782(2)
b/Å	12.1155(7)	12.0266(3)	12.0332(4)
c/Å	17.6748(10)	17.6197(4)	17.5540(6)
α/°	90	90	90
β/°	91.136(2)	90.8670(10)	90.652(2)
γ/°	90	90	90
Volume/Å^3	1223.31(12)	1206.36(5)	1199.33(7)
Z	4	4	4
ρ_{calc}g/cm^3	2.569	2.618	2.665
μ/mm^{-1}	12.716	13.558	15.071
F(000)	904.0	908.0	916.0
Radiation	CuKα (λ = 1.54178)	CuKα (λ = 1.54178)	CuKα (λ = 1.54178)
2Θ range for data collection/°	10.01 to 140.308	10.042 to 143.402	10.078 to 143.992
Reflections collected	11086	14549	20269
Independent reflections	2228 [R_{int} = 0.0486, R_{sigma} = 0.0272]	2115 [R_{int} = 0.0186, R_{sigma} = 0.0116]	2318 [R_{int} = 0.0274, R_{sigma} = 0.0145]
Goodness-of-fit on F^2	1.078	1.106	1.079
Final R indexes [I>=2σ (I)]	R_1 = 0.0411, wR_2 = 0.0984	R_1 = 0.0246, wR_2 = 0.0635	R_1 = 0.0207, wR_2 = 0.0518
Final R indexes [all data]	R_1 = 0.0415, wR_2 = 0.0990	R_1 = 0.0246, wR_2 = 0.0635	R_1 = 0.0209, wR_2 = 0.0519

Table S3. Crystal data and structure refinement for Ce-**Cy** (series 3).

Identification code	**Ce-Cy**
Empirical formula	$C_6H_{14}CeN_7O_{10}$
CCDC number	2178358
Formula weight	484.36
Temperature/K	150
Crystal system	monoclinic
Space group	$P2_1/c$
a/Å	6.6711(4)
b/Å	19.7592(12)
c/Å	21.1063(13)
α/°	90
β/°	98.303(2)
γ/°	90
Volume/Å^3	2753.0(3)
Z	8
ρ_{calc}g/cm^3	2.337
μ/mm^{-1}	18.091
F(000)	1896.0
Radiation	GaKα (λ = 1.34139)
2Θ range for data collection/°	5.356 to 121.44
Index ranges	$-8 \leq h \leq 8$, $-25 \leq k \leq 25$, $-27 \leq l \leq 27$
Reflections collected	79204
Independent reflections	6336 [R_{int} = 0.0309, R_{sigma} = 0.0125]
Data/restraints/parameters	6336/0/448
Goodness-of-fit on F^2	1.081
Final R indexes [I>=2σ (I)]	R_1 = 0.0188, wR_2 = 0.0502
Final R indexes [all data]	R_1 = 0.0195, wR_2 = 0.0506

Table S4. Crystal data and structure refinement for La-**Cy** (series 4).

Identification code	**La-Cy**
Empirical formula	$C_6H_{14}LaN_7O_{10}$
CCDC number	2178357
Formula weight	483.15
Temperature/K	100
Crystal system	orthorhombic
Space group	$I2_12_12_1$
a/Å	6.5379(2)
b/Å	10.6082(3)
c/Å	19.3914(6)
α/°	90
β/°	90
γ/°	90
Volume/Å^3	1344.90(7)
Z	4
ρ_{calc}g/cm^3	2.386
μ/mm^{-1}	17.378
F(000)	944.0
Radiation	GaKα (λ = 1.34139)
2Θ range for data collection/°	7.934 to 109.854
Reflections collected	11301
Independent reflections	1269 [R_{int} = 0.0309, R_{sigma} = 0.0157]
Goodness-of-fit on F^2	1.095
Final R indexes [I>=2σ (I)]	R_1 = 0.0403, wR_2 = 0.0992
Final R indexes [all data]	R_1 = 0.0403, wR_2 = 0.0993

Table S5. Effective ionic radii (Å) of Ln $^{3+}$ ions with corresponding coordination number (Shannon-Prewitt data).

Ln-Cy series	Ln ion	Effective ionic radii (Å)	Charge density (C.mm^{-3})	Coordination number (CN)
3	La^{3+}	1.270	72	10
4	Ce^{3+}	1.196	75	9
1	Pr^{3+}	1.179	79	9
	Sm^{3+}	1.132	86	
	Eu^{3+}	1.120	88	
	Gd^{3+}	1.107	91	
	Tb^{3+}	1.095	96	
	Dy^{3+}	1.083	99	
2	Ho^{3+}	1.015	102	8
	Er^{3+}	1.004	105	
	Tm^{3+}	0.994	108	
	Yb^{3+}	0.985	111	

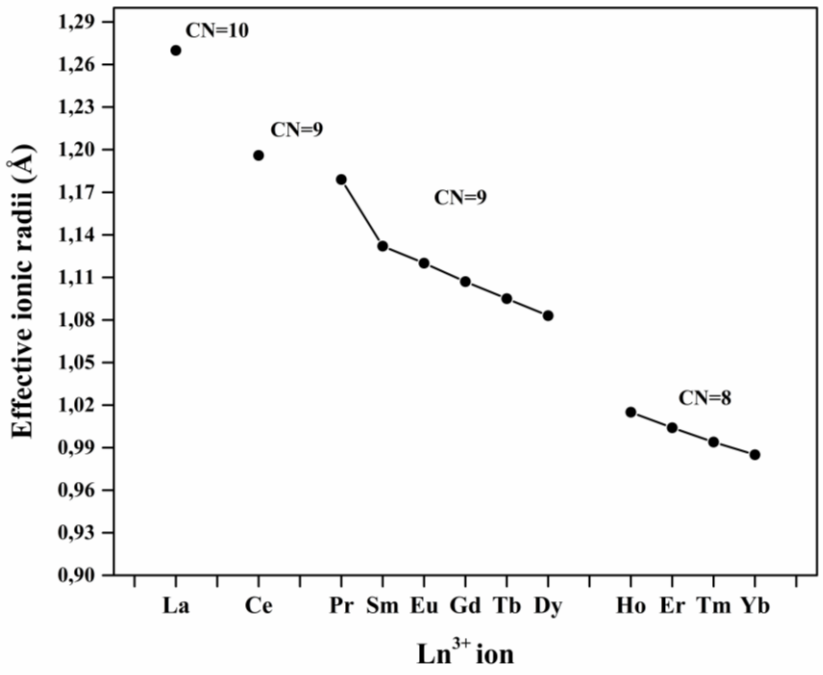

Figure S5. Effective ionic radius (Å) vs Ln^{3+} ions (cn = coordination number).

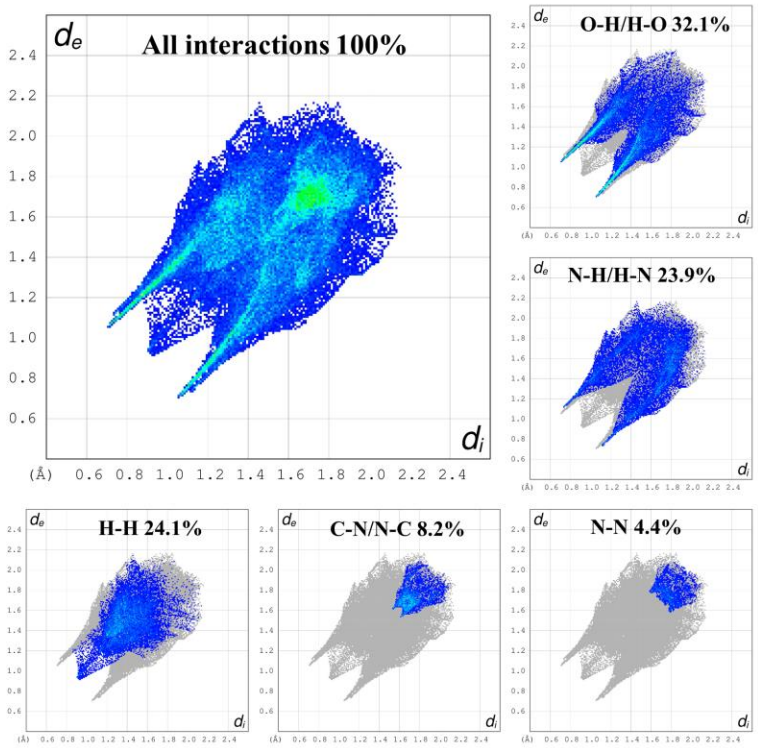

Figure S6. Two-dimensional fingerprint plots of the Ln-**Cy** series 1.

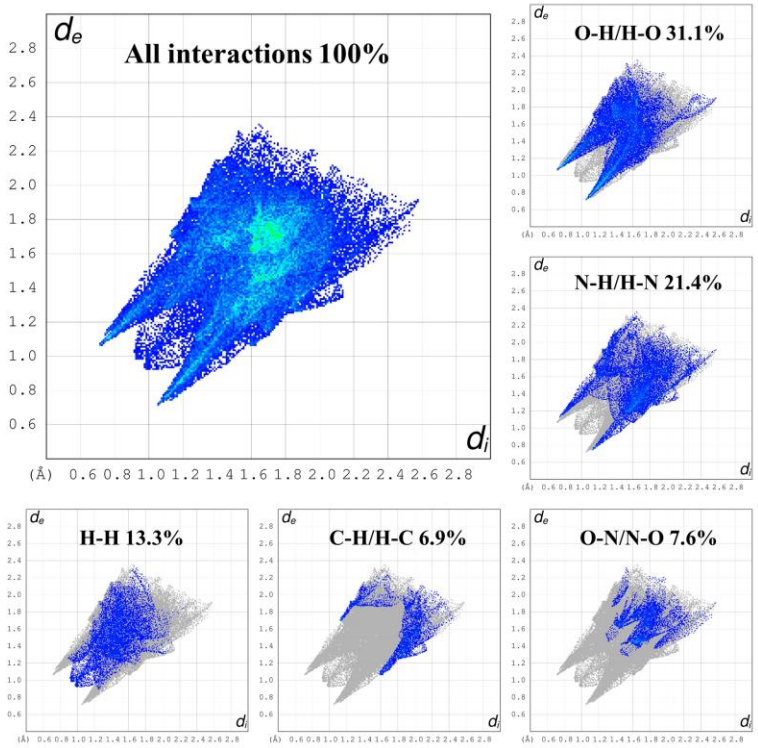

Figure S7. Two-dimensional fingerprint plots of Ln-**Cy** series 2.

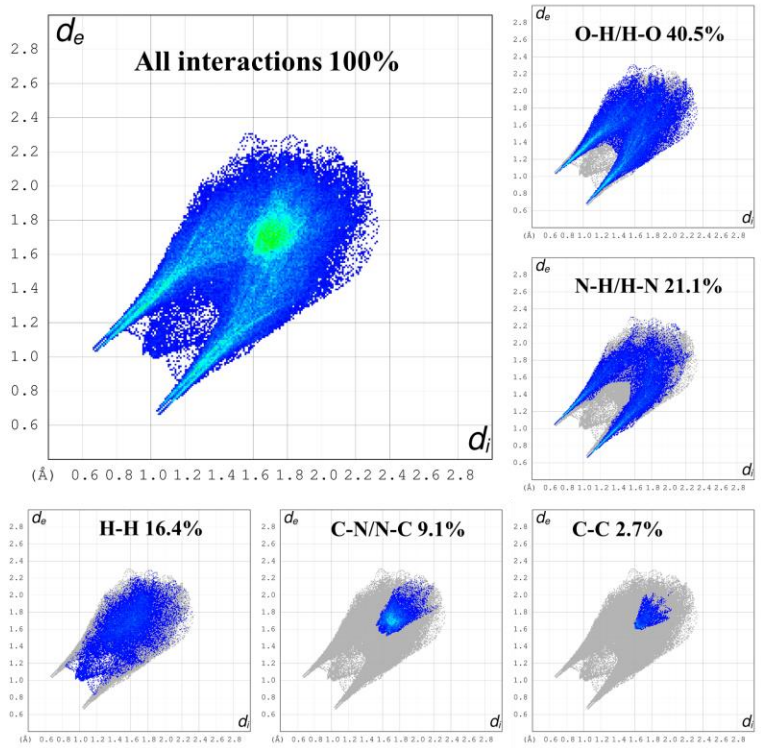

Figure S8. Two-dimensional fingerprint plots of Ln-**Cy** series 3.

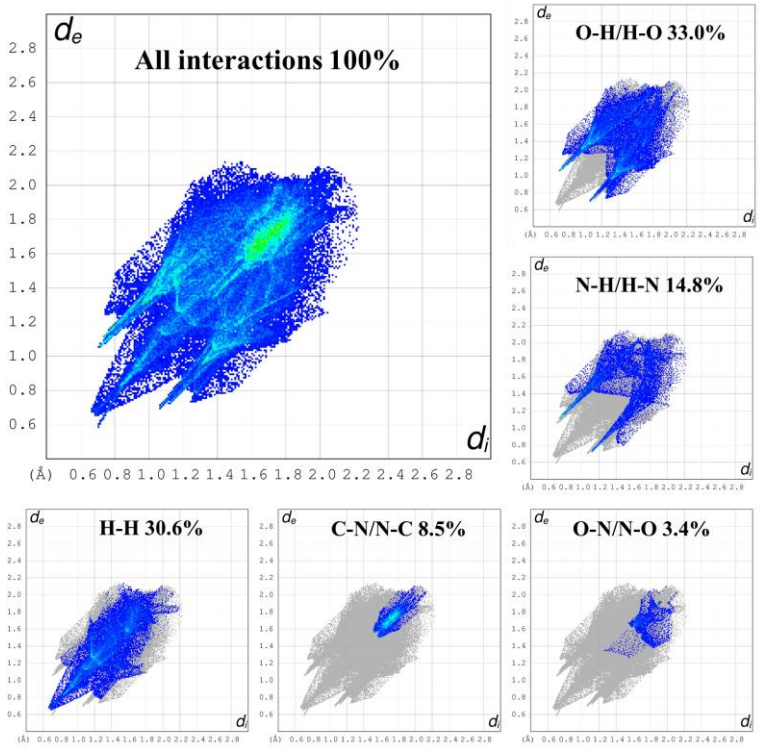

Figure S9. Two-dimensional fingerprint plots of Ln-**Cy** series 4.

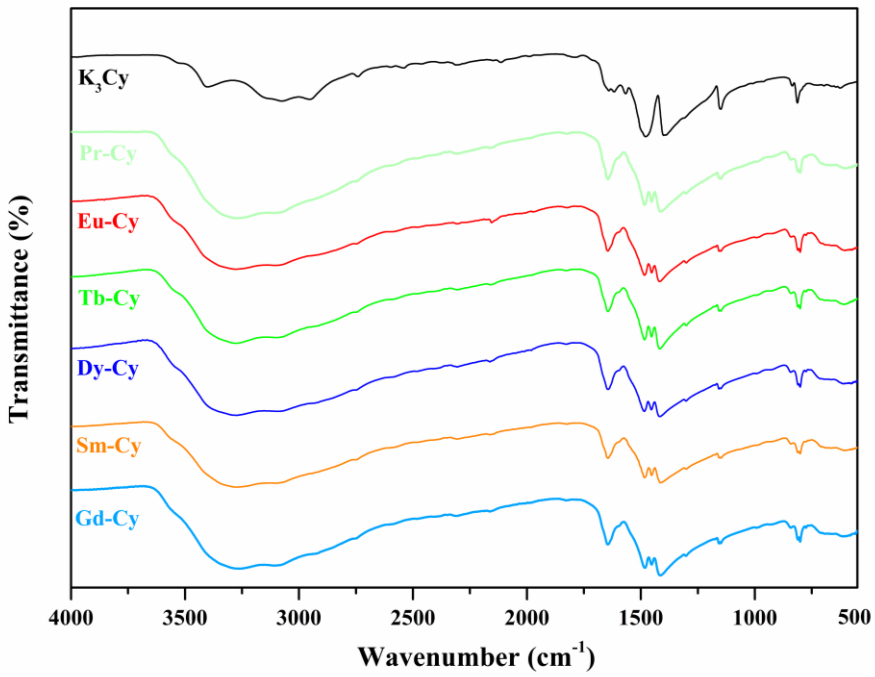

Figure S10. FTIR spectra of Ln-**Cy** series 1 in comparison with potassium cyamelurate.

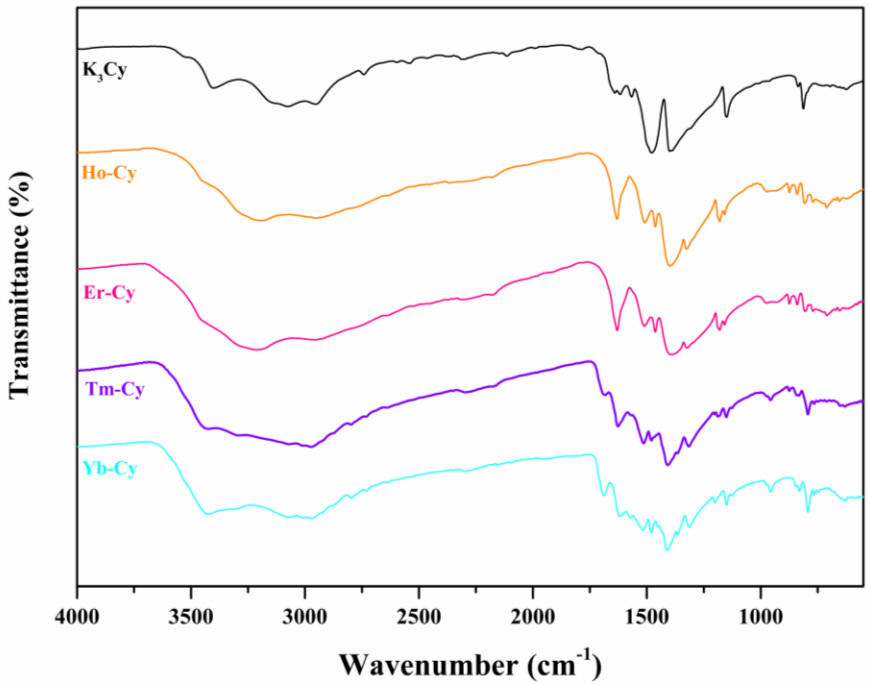

Figure S11. FTIR spectra of Ln-**Cy** series 2 in comparison with potassium cyamelurate.

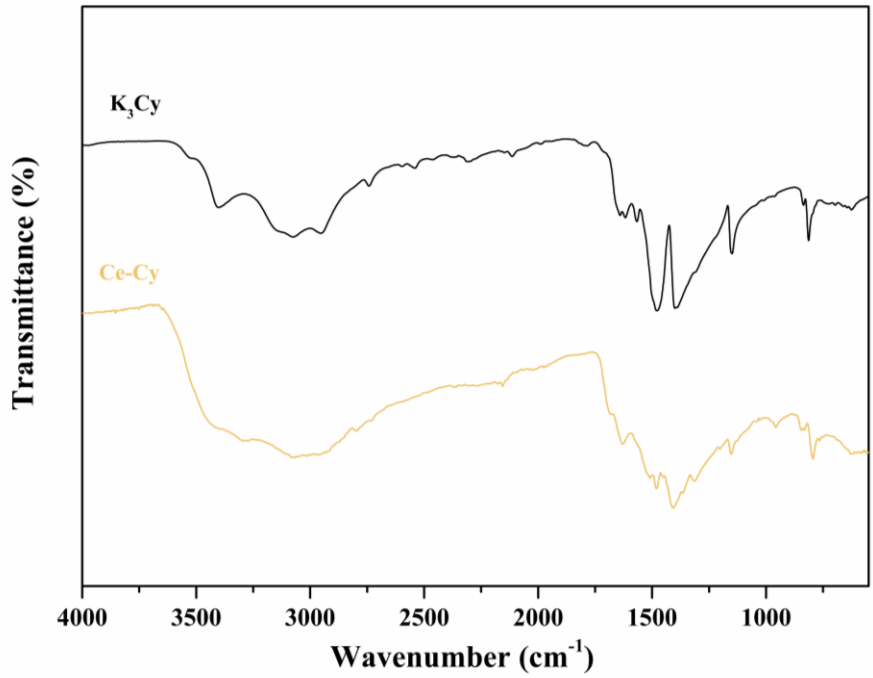

Figure S12. FTIR spectra of Ln-**Cy** series 3 in comparison with potassium cyamelurate.

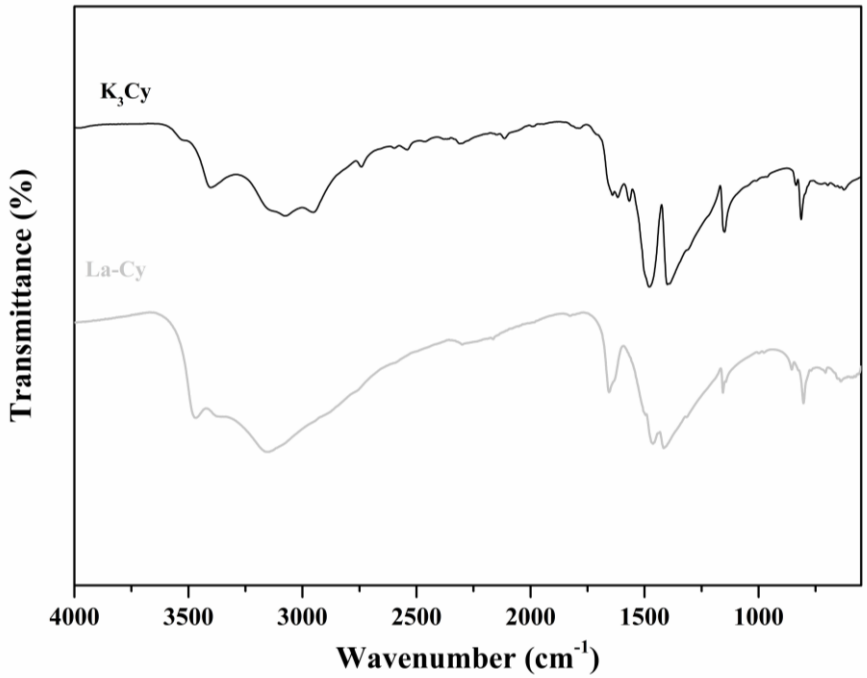

Figure S13. FTIR spectra of Ln-**Cy** series 4 in comparison with potassium cyamelurate.

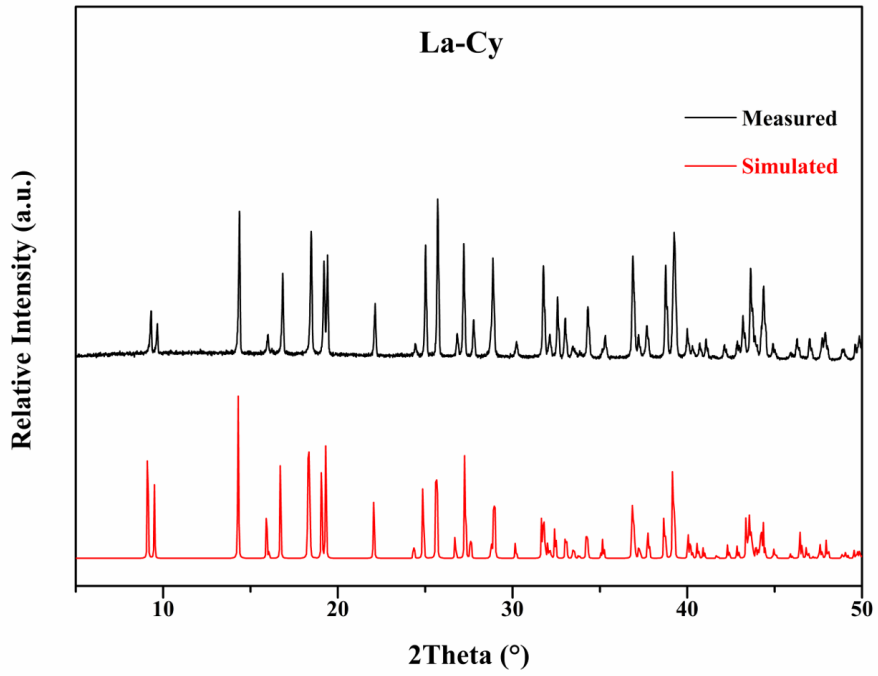

Figure S14. Experimental and simulated PXRD patterns for La-**Cy** compound.

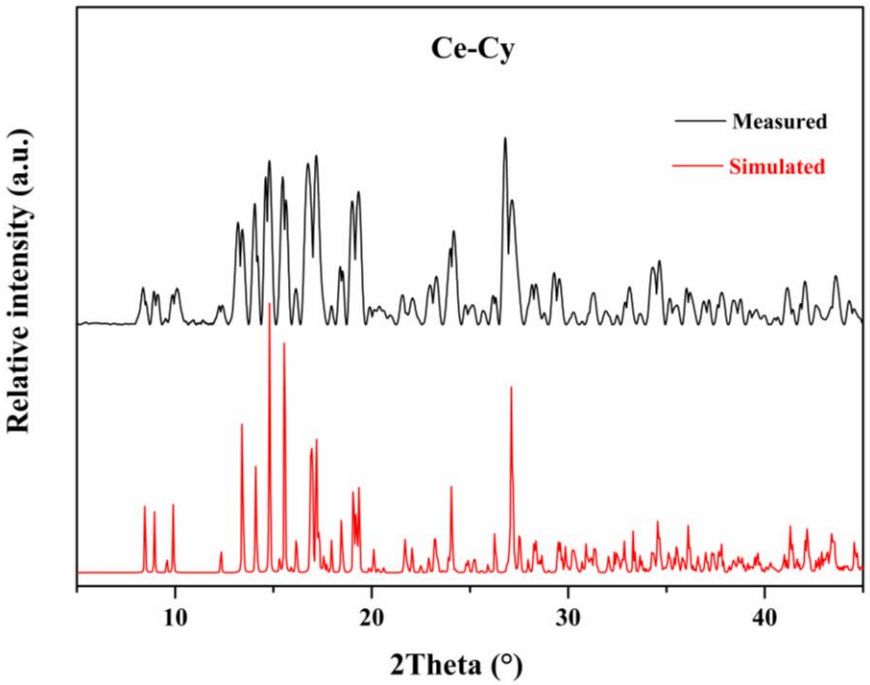

Figure S15. Experimental and simulated PXRD patterns for Ce-**Cy** compound.

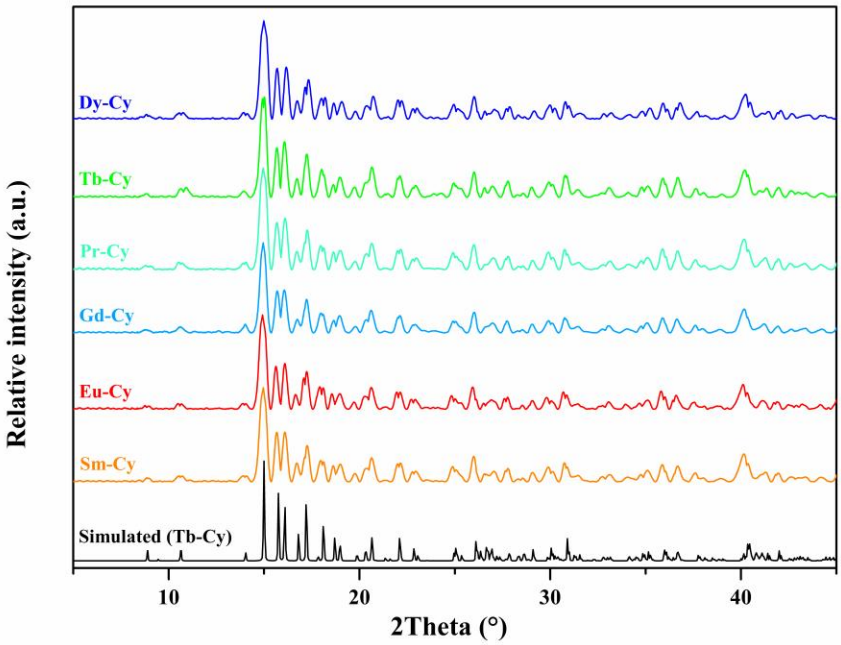

Figure S16. Experimental and simulated PXRD patterns for Ln-**Cy** series 1.

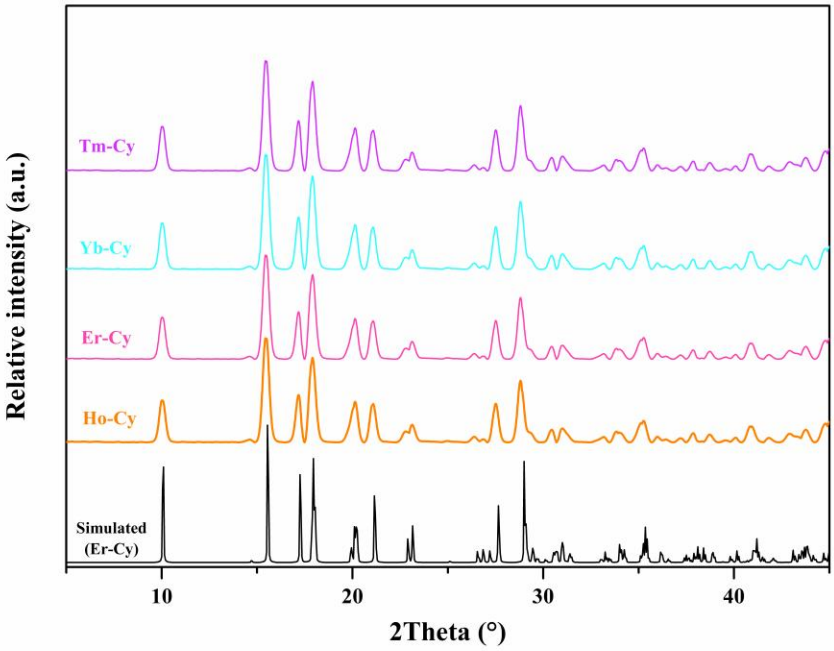

Figure S17. Experimental and simulated PXRD patterns for Ln-**Cy** series 2.

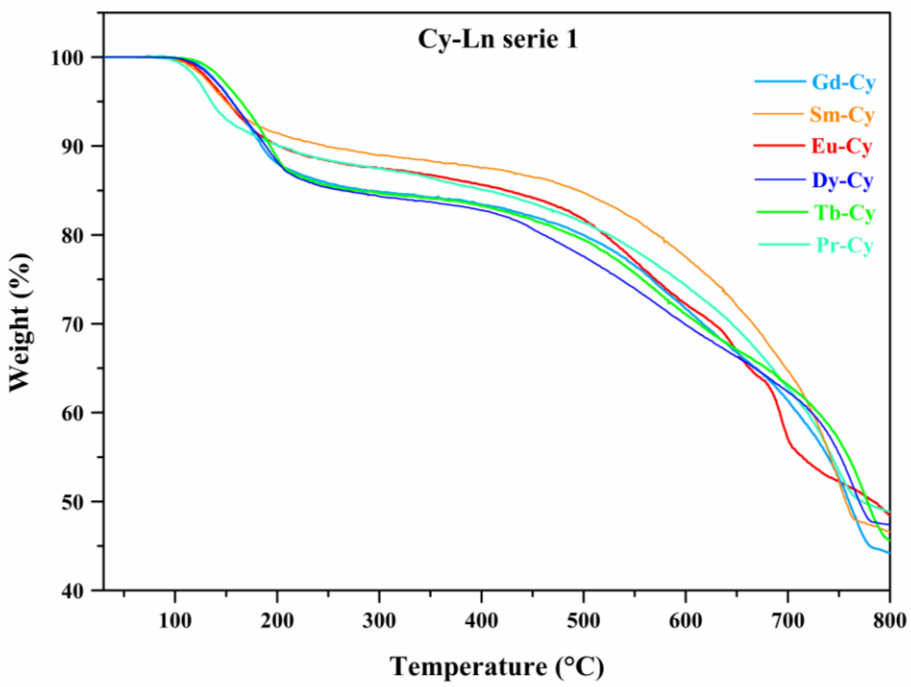

Figure S18. Thermogravimetric analysis curves for Ln-**Cy** series 1.

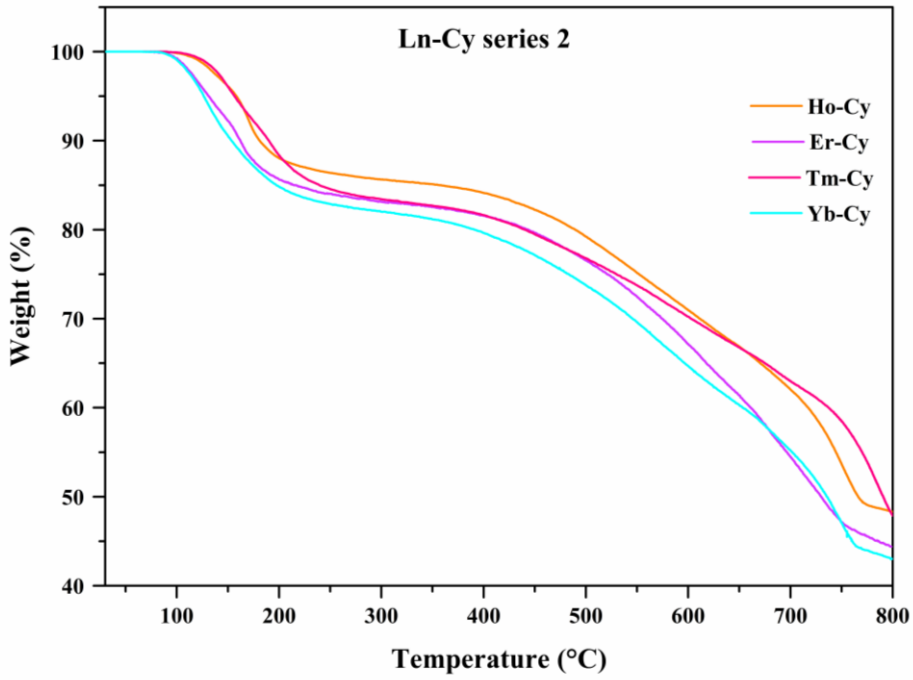

Figure S19. Thermogravimetric analysis curves for Ln-**Cy** series 2.

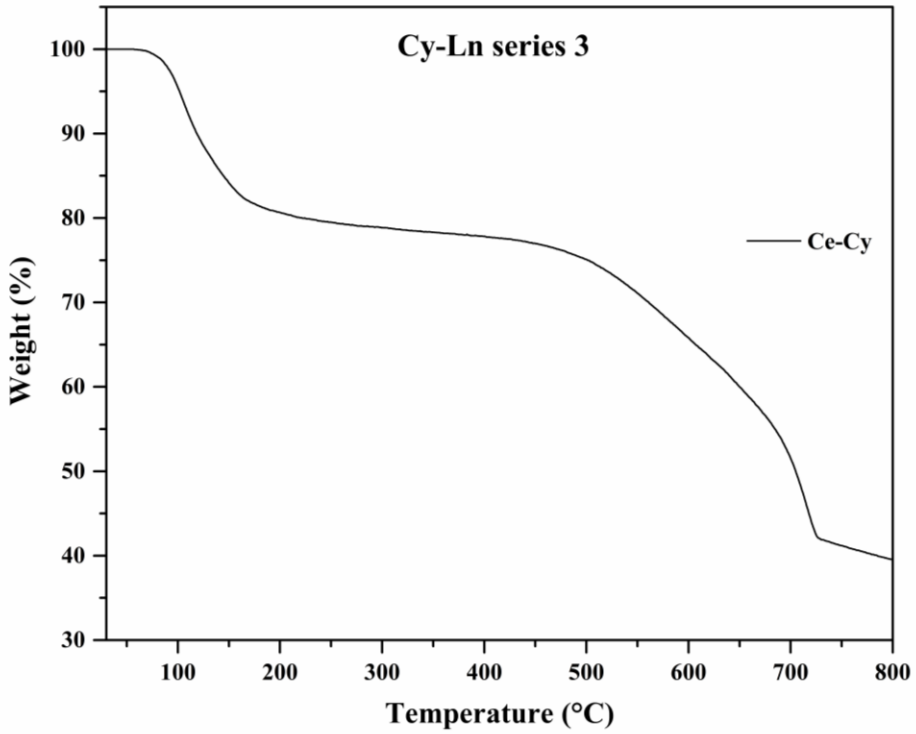

Figure S20. Thermogravimetric analysis curve for Ln-**Cy** series 3.

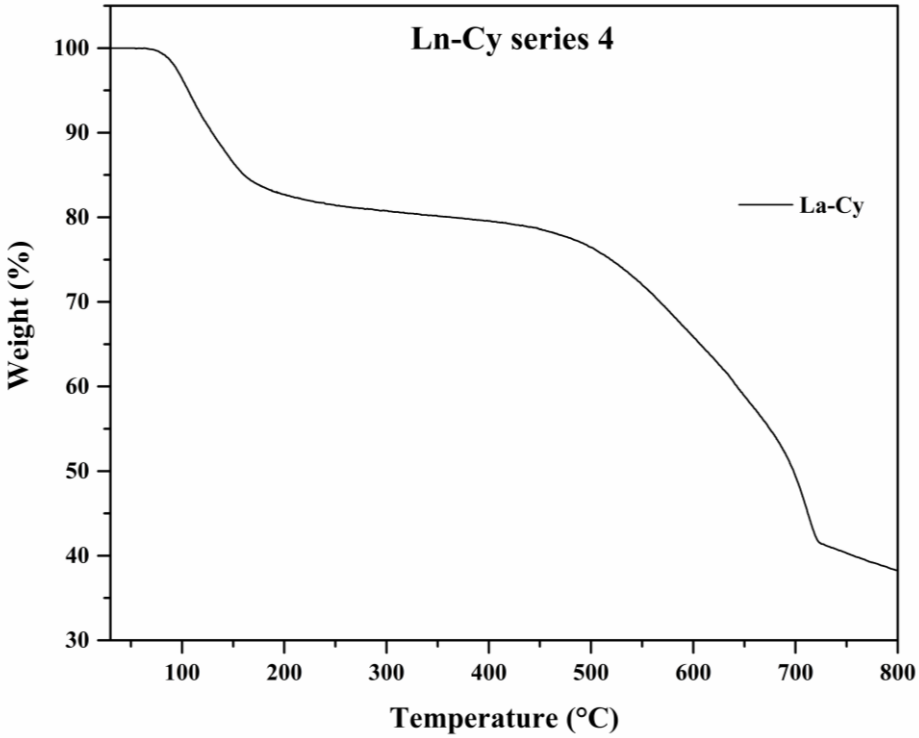

Figure S21. Thermogravimetric analysis curve for Ln-**Cy** series 4.

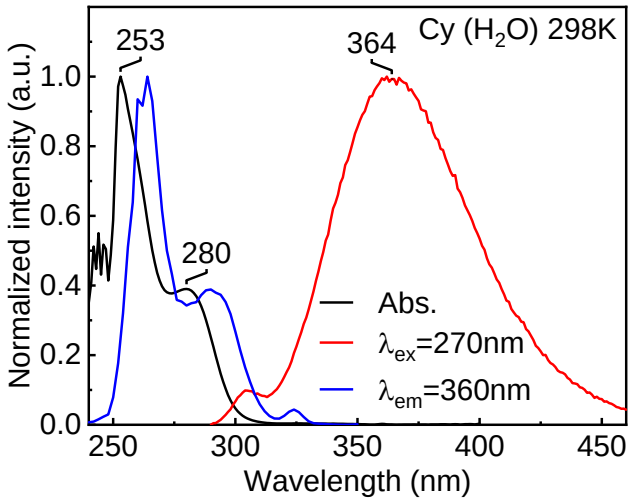

Figure S22. Absorption (black), emission (red) and excitation (blue) spectra for K_3**Cy** in solution in water at 298 K (λ_{ex} = 270 nm, λ_{em} = 364 nm). The weak signal at ~305 nm is suspected to be fluorescence, and the large and intense one centered at 364 nm is assigned to a triplet emission. Unfortunately, the ligand decomposes upon laser exposure at 266 nm, so the fluorescence lifetime is not accessible.

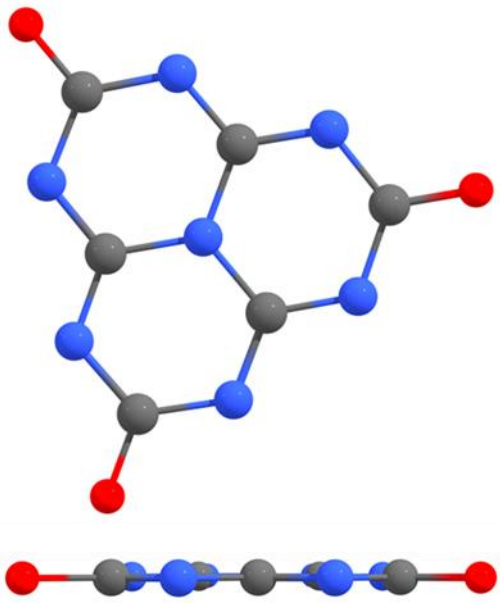

Figure S23. Side and front view of geometry optimization for $\mathbf{Cy}^{3-}$ anion in the gas phase.

Table S6. Cartesian coordinates (Å) of the geometry optimized $\mathbf{Cy}^{3-}$ in the gas phase.

Atoms	X	Y	Z
N	-0.616832047104	4.593426455720	10.643241677131
N	-2.392938011823	4.179950631859	12.175222354486
N	-2.601393328827	5.897099191815	10.457273921951
N	-0.850536754913	6.277494976359	8.975304675126
N	1.194261540371	4.960235032302	9.140301135928
N	1.392707332124	3.321883430688	10.778282948480
N	-0.443605631222	2.922080382750	12.331305935801
O	1.503605907509	1.736624383553	12.415036752309
O	-4.268256069265	5.459625132085	11.951980835584
O	0.914746741299	6.585211070393	7.563679330435
C	-1.164439084449	3.881151730106	11.743329421367
C	-3.110839886592	5.184571683521	11.536714492874
C	-1.374686841214	5.614201193252	10.009908851508
C	0.429182880429	5.953775768550	8.540049561437
C	0.688544242850	4.284265570210	10.175829308703
C	0.831078298913	2.641808627374	11.852851066965

Table S7. Calculated position, oscillator strength (f) and major contributions (%) of the first 100 singlet-singlet electronic transitions for $\mathbf{Cy}^{3-}$ in the gas phase.

N°.	**λ (nm)**	**f**	**Major contributions (%)**
1	289	0	HOMO→LUMO (97%)
2	257	0	H-3→LUMO (90%)
3	248	0	H-5→LUMO (11%), H-4→LUMO (19%), H-3→L+1 (57%)
4	248	0	H-5→LUMO (20%), H-4→LUMO (11%), H-3→L+2 (56%)
5	246	0.0464	HOMO→L+1 (87%)
6	246	0.0463	HOMO→L+2 (87%)
7	244	0	H-4→LUMO (42%), H-3→L+1 (16%)
8	244	0	H-5→LUMO (42%), H-3→L+2 (16%)
9	241	0	H-6→LUMO (70%)
10	235	0.0092	H-5→L+1 (32%), H-5→L+2 (14%), H-4→L+1 (14%), H-4→L+2 (32%)
11	234	0	H-8→LUMO (38%), H-6→L+1 (16%)
12	234	0	H-9→LUMO (38%), H-6→L+2 (15%)
13	231	0.05	H-2→L+1 (10%), H-1→LUMO (74%), H-1→L+2 (10%)
14	231	0.05	H-2→LUMO (74%), H-2→L+2 (10%), H-1→L+1 (10%)
15	229	0	H-2→L+1 (47%), H-1→L+2 (47%)
16	224	0	H-5→L+1 (24%), H-4→LUMO (14%), H-4→L+2 (24%), H-3→L+1 (10%)
17	224	0	H-5→LUMO (14%), H-5→L+2 (24%), H-4→L+1 (24%),

			H-3→L+2 (10%)
18	221	0	H-2→L+2 (45%), H-1→L+1 (44%)
19	221	0	H-6→LUMO (12%), H-5→L+1 (11%), H-5→L+2 (26%), H-4→L+1 (26%), H-4→L+2 (12%)
20	216	0.0348	H-7→L+1 (46%), H-2→L+1 (19%), H-1→L+2 (20%)
21	216	0.0351	H-7→L+2 (46%), H-2→L+2 (20%), H-1→L+1 (19%)
22	215	0	H-9→L+1 (11%), H-8→L+2 (11%), H-6→L+1 (63%)
23	215	0	H-9→L+2 (11%), H-8→L+1 (11%), H-6→L+2 (63%)
24	211	$3E^{-4}$	H-9→L+1 (34%), H-9→L+2 (13%), H-8→L+1 (13%), H-8→L+2 (34%)
25	205	0	H-9→L+1 (11%), H-9→L+2 (26%), H-8→L+1 (29%), H-8→L+2 (10%), H-6→LUMO (16%)
26	205	0	H-9→L+1 (20%), H-9→L+2 (10%), H-8→LUMO (26%), H-8→L+1 (10%), H-8→L+2 (19%)
27	205	0	H-9→LUMO (25%), H-9→L+2 (21%), H-8→L+1 (18%), H-8→L+2 (10%)
28	201	0	H-7→LUMO (88%)
29	197	0.9068	H-7→L+1 (43%), H-2→L+1 (13%), H-1→LUMO (20%), H-1→L+2 (13%)
30	197	0.9064	H-7→L+2 (43%), H-2→LUMO (20%), H-2→L+2 (13%), H-1→L+1 (13%)
31	180	0	H-10→LUMO (78%)
32	180	0	H-11→LUMO (78%)
33	174	0.0033	H-12→LUMO (41%), H-11→L+1 (29%), H-10→L+2 (29%)
34	174	0	H-11→L+2 (49%), H-10→L+1 (49%)
35	170	0	H-11→LUMO (13%), H-11→L+2 (36%), H-10→L+1 (36%)
36	170	0	H-11→L+1 (36%), H-10→LUMO (13%), H-10→L+2 (36%)
37	164	$3E^{-4}$	H-12→LUMO (57%), H-11→L+1 (21%), H-10→L+2 (21%)
38	163	0	H-12→L+1 (87%)
39	163	0	H-12→L+2 (87%)
40	153	$8E^{-4}$	HOMO→L+3 (90%)
41	153	$8E^{-4}$	HOMO→L+4 (90%)
42	152	0	H-3→L+3 (59%), H-3→L+4 (22%)
43	152	0	H-3→L+3 (22%), H-3→L+4 (59%)
44	150	0	H-14→L+1 (47%), H-13→L+2 (47%)
45	150	0.0045	H-13→LUMO (80%)
46	150	0.0045	H-14→LUMO (80%)
47	148	0	H-5→L+3 (46%), H-4→L+4 (46%)
48	146	0	H-6→L+4 (33%), H-5→L+3 (24%), H-4→L+4 (24%)
49	146	0	H-6→L+3 (33%), H-5→L+4 (24%), H-4→L+3 (24%)

50	145	0.0163	H-14→L+1 (21%), H-13→L+2 (21%), H-2→L+4 (11%), H-1→L+3 (11%)
51	145	0.0163	H-14→L+2 (20%), H-13→L+1 (21%), H-2→L+3 (11%), H-1→L+4 (11%)
52	145	0	H-9→L+3 (44%), H-8→L+4 (44%)
53	144	0	H-14→L+2 (14%), H-13→L+1 (14%), H-2→L+3 (29%), H-1→L+4 (29%)
54	143	0	H-2→L+4 (42%), H-1→L+3 (44%)
55	143	0.0061	H-5→L+4 (46%), H-4→L+3 (47%)
56	143	$2E^{-4}$	H-14→L+1 (14%), H-13→L+2 (14%), H-2→L+4 (22%), H-1→L+3 (20%)
57	143	$2E^{-4}$	H-14→L+2 (14%), H-13→L+1 (14%), H-2→L+3 (21%), H-1→L+4 (21%)
58	142	0	H-6→L+3 (27%), H-5→L+4 (11%), H-4→L+3 (11%)
59	142	0	H-6→L+4 (27%), H-5→L+3 (11%), H-4→L+4 (11%)
60	140	0	H-14→L+2 (31%), H-13→L+1 (31%), H-2→L+3 (11%), H-1→L+4 (11%)
61	137	0.008	H-15→L+1 (20%), H-7→L+3 (31%), H-7→L+4 (43%)
62	137	0.008	H-15→L+2 (20%), H-7→L+3 (43%), H-7→L+4 (31%)
63	136	0	H-9→L+4 (29%), H-8→L+3 (30%), H-6→L+3 (29%)
64	136	0	H-9→L+3 (30%), H-8→L+4 (30%), H-6→L+4 (29%)
65	134	$1E^{-4}$	H-9→L+4 (48%), H-8→L+3 (47%)
66	134	0	H-15→LUMO (90%)
67	133	0	HOMO→L+5 (99%)
68	132	0.0087	H-15→L+1 (65%), H-7→L+4 (12%)
69	132	0.0088	H-15→L+2 (65%), H-7→L+3 (12%)
70	131	0	H-17→LUMO (10%), H-16→LUMO (65%)
71	131	0	H-17→LUMO (65%), H-16→LUMO (10%)
72	127	0.0083	H-20→LUMO (32%), H-17→L+2 (25%), H-16→L+1 (25%)
73	126	0	H-17→L+1 (38%), H-17→L+2 (11%), H-16→L+1 (11%), H-16→L+2 (37%)
74	126	0	HOMO→L+6 (84%)
75	124	0	H-17→L+1 (33%), H-16→L+2 (34%)
76	124	0	H-17→L+2 (34%), H-16→L+1 (34%)
77	124	0	H-1→L+5 (83%)
78	124	0	H-2→L+5 (84%)
79	124	0	H-3→L+5 (89%)
80	121	0.0127	H-19→LUMO (13%), H-18→LUMO (28%), H-5→L+5 (20%), H-4→L+5 (30%)
81	121	0.0126	H-19→LUMO (28%), H-18→LUMO (14%), H-5→L+5 (30%), H-4→L+5 (20%)
82	121	0	H-3→L+6 (64%)
83	121	0.0172	H-11→L+3 (10%), H-11→L+4 (38%), H-10→L+3 (38%),

			H-10→L+4 (10%)
84	121	0.0022	H-18→LUMO (39%), H-5→L+5 (15%), H-4→L+5 (10%)
85	121	0.0023	H-19→LUMO (39%), H-5→L+5 (10%), H-4→L+5 (15%)
86	121	0	H-12→L+4 (13%), H-11→L+3 (28%), H-10→L+4 (28%)
87	121	0	H-12→L+3 (13%), H-11→L+4 (28%), H-10→L+3 (28%)
88	119	0.0089	H-19→L+1 (16%), H-19→L+2 (19%), H-18→L+1 (21%), H-18→L+2 (14%), H-5→L+5 (15%)
89	119	0.0089	H-19→L+1 (20%), H-19→L+2 (15%), H-18→L+1 (15%), H-18→L+2 (20%), H-4→L+5 (15%)
90	119	0	H-19→L+1 (15%), H-19→L+2 (22%), H-18→L+1 (20%), H-18→L+2 (16%), H-6→L+5 (12%)
91	119	0.0019	H-20→LUMO (64%), H-17→L+2 (13%), H-16→L+1 (13%)
92	118	0	H-20→L+1 (33%), H-5→L+6 (29%), H-4→L+6 (10%)
93	118	0	H-20→L+2 (32%), H-5→L+6 (10%), H-4→L+6 (29%)
94	118	0	H-19→L+1 (27%), H-19→L+2 (20%), H-18→L+1 (20%), H-18→L+2 (27%)
95	118	0	H-3→L+6 (18%), HOMO→L+7 (60%)
96	118	0.0088	H-1→L+6 (88%)
97	118	0.0088	H-2→L+6 (88%)
98	118	0	H-20→L+1 (56%), H-5→L+6 (20%)
99	118	0	H-20→L+2 (57%), H-4→L+6 (20%)
100	117	0.0039	H-7→L+5 (97%)

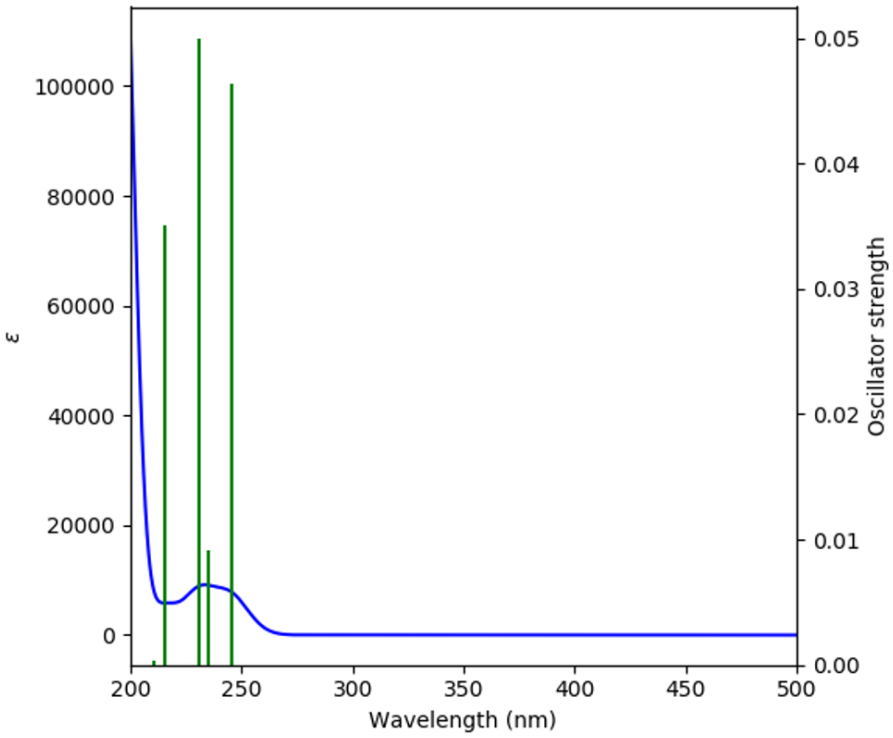

Figure S24. Simulated absorption spectrum for **Cy**$^{3-}$ in the gas phase by TDDFT computations. Bar graph reporting the calculated oscillator strength and the calculated position of the 100th electronic transitions calculated by TDDFT for **Cy**$^{3-}$ in the gas phase (bar graph; f = computed oscillator strength).

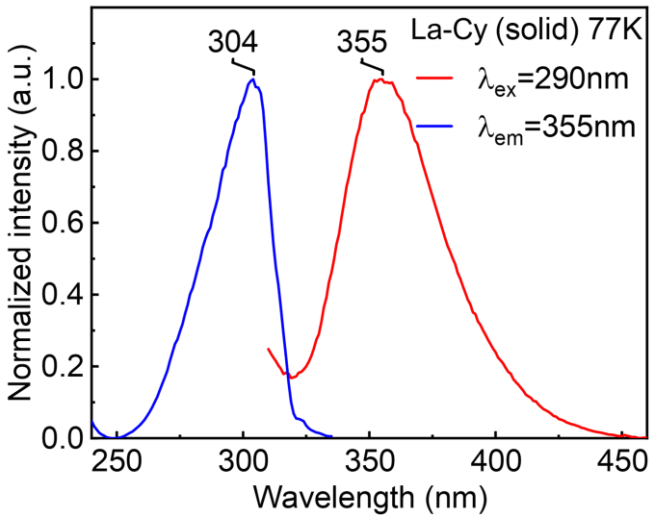

Figure S25. Solid-state absorption (black), emission (red) and excitation (blue) spectra for La-**Cy** at 298 K (λ_{ex} = 270 nm, λ_{em} = 335 nm) and 77K (λ_{ex} = 270 nm, λ_{em} = 355 nm).

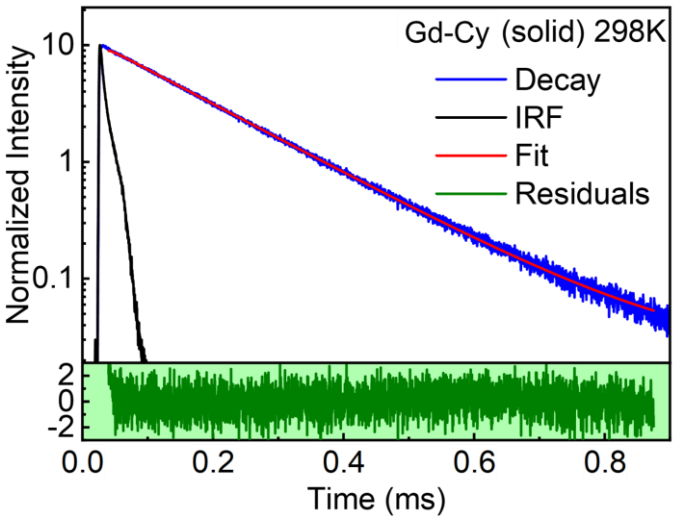

Figure S26. Decay of emission intensity, fit, IRF and residual of Gd-**Cy** at 298 K. λ = 339 nm (λ_{ex} = 277 nm), τ_e {f%} = 15 μs {100}, χ^2 = 1.070.

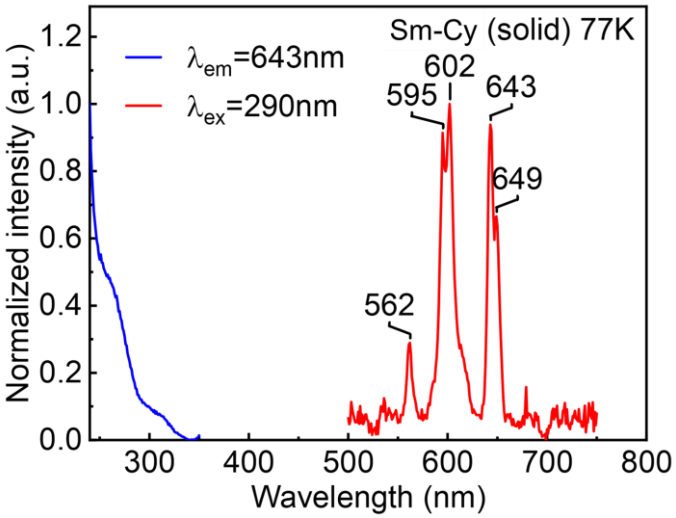

Figure S27. Solid-state absorption (black), emission (red) and excitation (blue) spectra for Sm-**Cy** at 77K (λ_{ex} = 290 nm, λ_{em} = 643 nm).

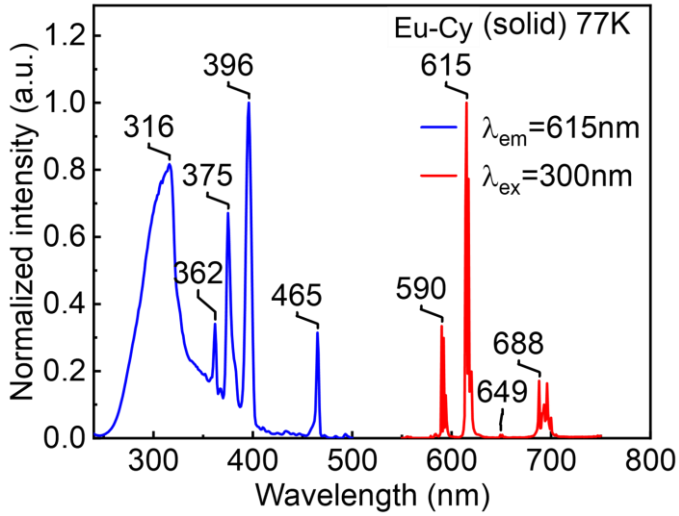

Figure S28. Solid-state absorption (black), emission (red) and excitation (blue) spectra for Eu-**Cy** at 77K (λ_{ex} = 300 nm, λ_{em} = 615 nm).

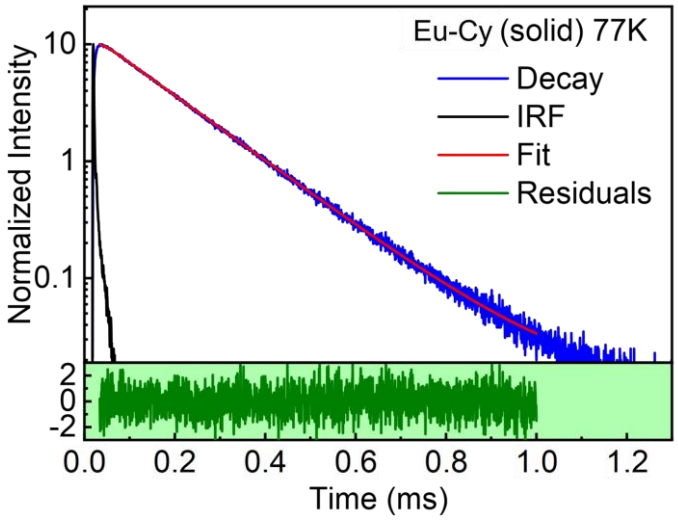

Figure S29. Decay of emission intensity, fit, IRF and residual of Eu-**Cy**. Left at 77 K λ = 615 nm (λ_{ex} = 300 nm), τ_e {f%} = 16 μs {100}, χ^2 = 1.001.

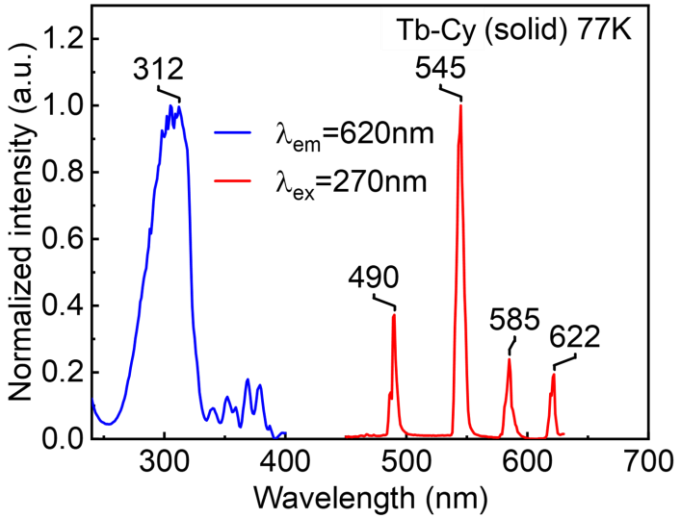

Figure S30. Solid-state absorption (black), emission (red) and excitation (blue) spectra for Tb-**Cy** at 77K (λ_{ex} = 270 nm, λ_{em} = 620 nm).

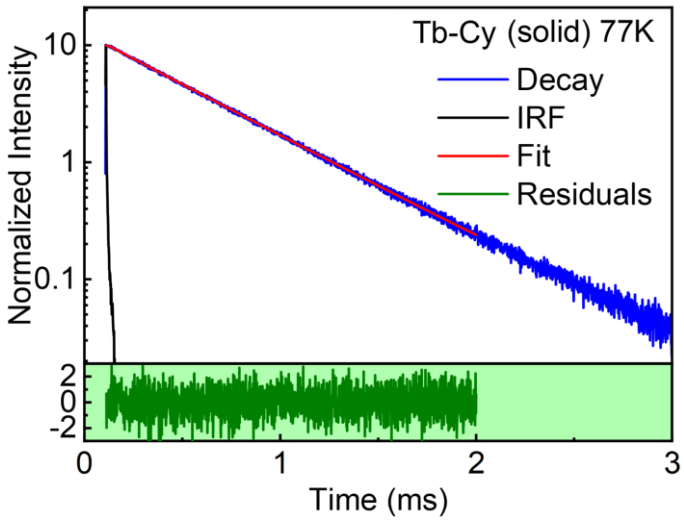

Figure S31. Decay of emission intensity, fit, IRF and residual of Tb-**Cy**. Left, at 77 K λ = 620 nm (λ_{ex} = 270 nm), τ_e {f%} = 50 μs {100}, χ^2 = 1.031.

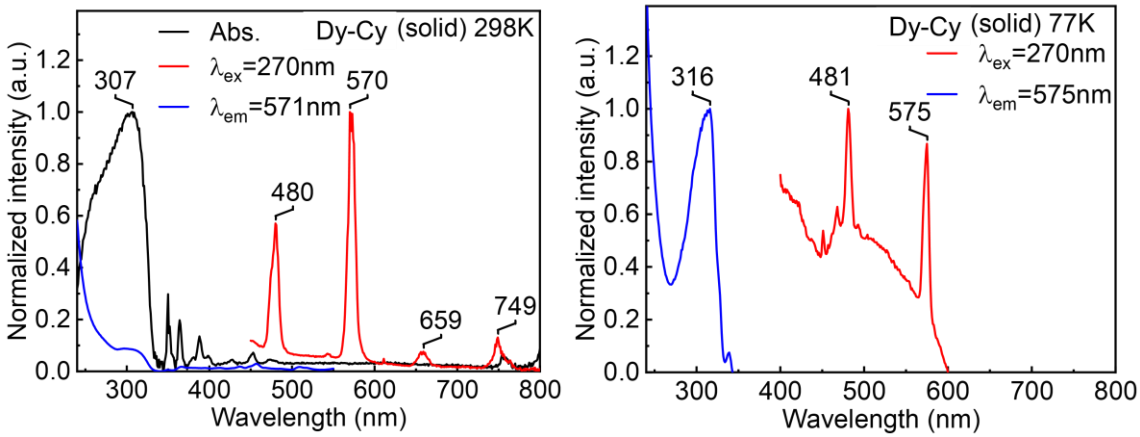

Figure S32. Solid-state absorption (black), emission (red) and excitation (blue) spectra for Dy-**Cy** at 298 K (λex = 270 nm, λem = 571 nm) and 77K (λex = 270 nm, λem = 575 nm).

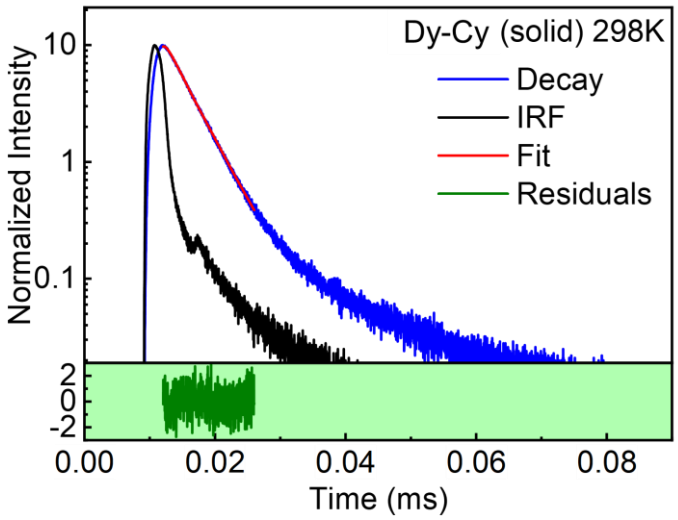

Figure S33. Decay of emission intensity, fit, IRF and residual of Dy-**Cy** at 298 K. λ = 570 nm (λ_{ex} = 270 nm), τ_e {f%} = 3.48 μs {100}, χ^2 = 1.034.

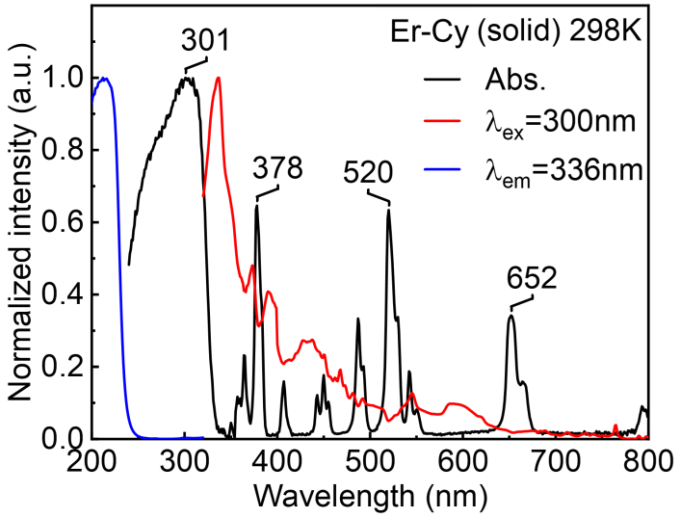

Figure S34. Solid-state absorption (black), emission (red) and excitation (blue) spectra for Er-**Cy** at 298 K (λ_{ex} = 300 nm, λ_{em} = 336 nm).

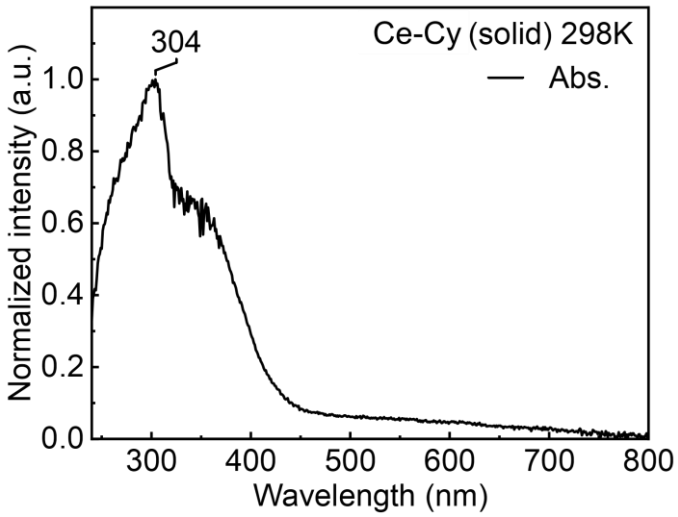

Figure S35. Solid-state absorption (black) spectra for Ce-**Cy** at 298 K.

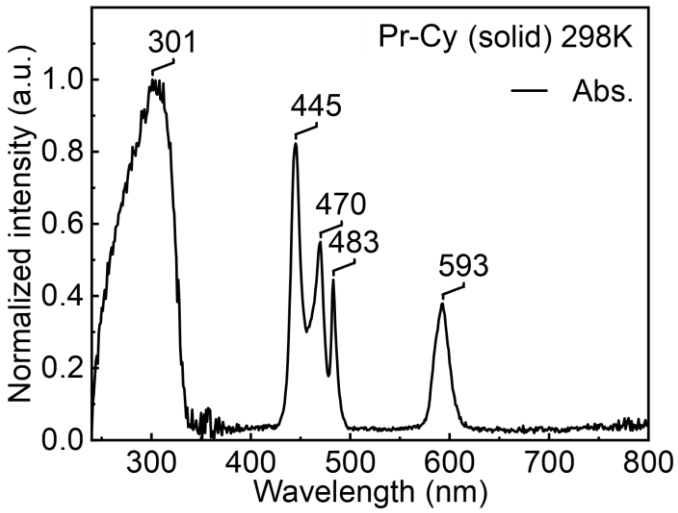

Figure S36. Solid-state absorption (black) spectra for Pr-**Cy-** at 298 K.

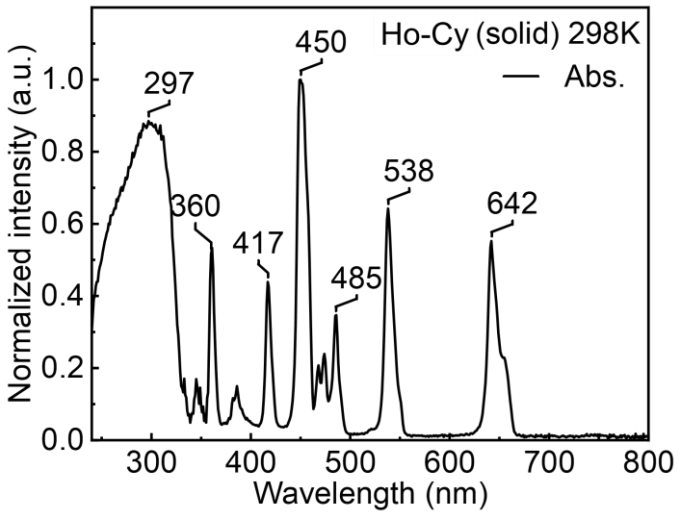

Figure S37. Solid-state absorption (black) for Ho-**Cy** at 298 K.

Table S8. Photophysical properties of all emissive Ln-**Cy**.

Photophysical series		**T(K)**	**λ_{ex} (nm)**	**λ_{em} (nm)**	**Corresponding transitions**	**τ_e {f%}**	**χ^2**
(A) only the ligand is emissive in the visible region	La-Cy	298	270	360	$\pi \rightarrow \pi^*$	3.3 µs {67.80}, 76.2 µs {32.20}	1.044
	Gd-Cy	298	277	339		15 µs {100}	1.070
	Tm-Cy	298	270	620		----	----
(B) both ligand and lanthanide metal are emissive in the visible region	Yb-Cy	298	270	328	$\pi \rightarrow \pi^*$ $^2F_{5/2} \rightarrow {}^2F_{7/2}$	----	----
(C) only the lanthanide metal is emissive in the visible region	Sm-Cy	298	310	641	$^4G_{5/2} \rightarrow {}^6H_{9/2}$	44.9 µs {6.4}, 270 µs {8.5}, 1.1 ms {16.3}, 4.0 ms {68.9}	1.072
	Eu-Cy	298	300	615	$^5D_0 \rightarrow {}^4F_2$	6.7 µs {2.37}, 150 µs {89.5}, 53 µs {8.1}	1.004
	Tb-Cy	298	270	545	$^5D_4 \rightarrow {}^4F_5$	49 µs {100}	1.021
	Dy-Cy	298	270	570	$^4F_{9/2} \rightarrow {}^6H_{13/2}$	3.48 µs {100}	1.034
	Er-Cy	298	300	336	$^4S_{3/2} \rightarrow {}^4I_{15/2}$	----	----